Cell Variational Information Bottleneck Network

Zhonghua Zhai Chen Ju Jinsong Lan Shuai Xiao*

Alibaba Group
{zhaizhonghua.zzh@taobao.com}

Abstract. In this work, we propose "Cell Variational Information Bottleneck Network (cellVIB)", a convolutional neural network using information bottleneck mechanism, which can be combined with the latest feedforward network architecture in an end-to-end training method. Our Cell Variational Information Bottleneck Network is constructed by stacking VIB cells, which generate feature maps with uncertainty. As layers going deeper, the regularization effect will gradually increase, instead of directly adding excessive regular constraints to the output layer of the model as in Deep VIB [3]. Under each VIB cell, the feedforward process learns an independent mean term and an standard deviation term, and predicts the Gaussian distribution based on them. The feedback process is based on reparameterization trick for effective training. This work performs an extensive analysis on MNIST dataset to verify the effectiveness of each VIB cells, and provides an insightful analysis on how the VIB cells affect mutual information. Experiments conducted on CIFAR-10 also prove that our cellVIB is robust against noisy labels during training and against corrupted images during testing. Then, we validate our method on PACS dataset, whose results show that the VIB cells can significantly improve the generalization performance of the basic model. Finally, in a more complex representation learning task, face recognition, our network structure has also achieved very competitive results.

1 Introduction

It is meaningful to explain deep neural networks from the perspective of information theory. The information bottleneck was first proposed in [37]. It is attractive because it makes a balance between the concise representation and the representation with good predictive ability [38]. The main disadvantage of the information bottleneck principle is that it is usually very difficult to calculate mutual information, which severely limits the types of learnable models and makes the information bottleneck only available under some extreme assumptions. For example, [37] uses the information bottleneck for clustering discrete data, and [4] uses the information bottleneck when the input, label and latent code all follow Gaussian distributions. To solve these problems, [3] uses variational inference to construct the lower bound of the information bottleneck optimization objective, and uses reparameterization trick [18] so that deep neural

* Corrsponding author, shuai.xsh@alibaba-inc.com

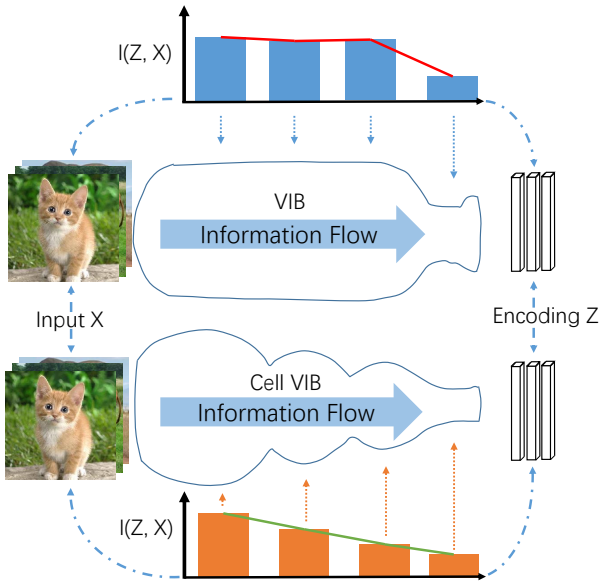

Fig. 1: Cell Variational Information Bottleneck. Best viewed in color.

networks can parameterize the distribution of high-dimensional continuous data and avoiding previous restrictions on discrete or Gaussian cases. However, the experiments in the recent literature [39] show that such information bottleneck methods are still not thorough enough.

To understand information theory from the perspective of regularization, the latent code Z of the input X is defined by the parameter encoder $P(Z|X;\theta)$. The target is to learn a code that can understand the target Y to the greatest extent, measured by the mutual information $I(Z,Y;\theta)$ between the code Z and the target Y, and at the same time, to minimize the complexity of Z, measured by the mutual information $I(Z,X;\theta)$ between code Z and input X. In order to improve the regularity effect, we penalize the redundant information theory measurement between adjacent network layers, that is, use variational approximation to penalize the mutual information between the layers, instead of only penalizing mutual information between Z and X. When looking at information theory from another perspective, uncertainty comes from two parts [2]. First, Z is no longer a certain point, but a random distribution; second, we penalize the KL divergence between the conditional distribution of a given input and a low-dimensional, low-information code space. In this case, for the upper bound of the variational inference of uncertainty, the layer-by-layer information interference is higher than just applying interference to a certain layer [39]. This is why we establish an information bottleneck in each cell (Figure 1).

The cellVIB network can be generated by simply stacking VIB cells, and VIB cells can also be used as a direct replacement for primitive blocks of any depth in the architecture. However, although the template of the cells is universal, there will still be differences in cells of different depths. In the shallow network, the VIB cell plays a weaker regularization role and introduces weaker uncertainty. As the network continues to deepen, the regularization and uncertainty will continue to strengthen. Therefore, the regularization and uncertainty of cellVIB

are gradual. The development of a new CNN architecture is a hard engineering task, usually involving many new layer configurations. In contrast, the design of the VIB cell outlined above is very convenient and can be used with the existing most advanced architectures directly. The modules of these architectures can be enhanced by directly replacing with the VIB cells.

In Section 4, we verify the superiority of cellVIB from different perspective. In order to further illustrate its general applicability, we have adopted different backbone structures and different datasets in different tasks to show that our proposed method is not limited to specific datasets or tasks. First, we analyze the correspondence between $I(Z;Y)$ and $I(Z;X)$ when β changes on MNIST dataset, and analyze how $I(Z;Y)$ and $I(Z;X)$ changes with the network depth. The experimental results demonstrate the deficiencies of Deep VIB in removing information redundancy. Subsequently, we also prove through a series of experiments that cellVIB method is robust to input noise and label noise, because the representation Z learned by cellVIB removes more redundant information about x. Besides, compared with the deterministic model fitted by maximum likelihood estimation or VIB, cellVIB has a stronger generalization ability. Intuitively speaking, each input image is mapped to a feature map distribution instead of a unique feature map in each layer. The introduction of this uncertainty strengthens the generalization ability of the model. Finally, our model also shows competitive results in the more challenging task: face recognition, a much more complex representation learning task.

2 Related work

Deep Architectures. VGGNets [30] and Inception models [35] explains the effect of network depth on performance. Batch normalization (BN) [15] improved the gradient propagation by inserting units for adjusting layer input, thereby stabilizing the learning process. ResNets [9, 10] demonstrated the effectiveness of learning deeper networks by using identity-based skip connections. Highway network [32] used a gating mechanism to adjust shortcut connections.

Another research direction is to explore ways to adjust the functional form of network modular components. Grouped convolution can be used to increase the cardinality [14, 43]. Multi-branch convolutions can be interpreted as a generalization of the concept, which makes the combination of operators more flexible [15, 34–36]. Recently, compositions learned in an automated manner [24, 47, 48] have shown competitive performance. Cross-channel correlation is usually independent of the spatial structure [5, 16] or by using a standard convolution filter with 1×1 convolution [23] to jointly map a new combination of features.

Regularization. There have been a large number of regularization techniques used to improve the generalization of deep neural networks [7, 15, 31], but we only discuss methods based on information theory regularizers and closely related to cell-VIB. Tishby & Zaslavsky [38] pointed out the idea of applying information theoretic objectives to deep neural networks. However, their work only contained theoretical hypotheses, and did not design experiments to verify

their hypotheses. Although not combined with the information bottleneck objective, variational bounds on mutual information has been discussed previously in [1]. Mohamed & Rezende [26] also explored variational bounds on mutual information and applied it for reinforcement learning. Variational autoencoder [18] is a special case in the unsupervised learning literature, in which the β parameter is fixed at 1.0 while Higgins et al. [12] explored VAE targets with different β values. Variational information bottleneck [3] suggests using variational inference to construct a lower bound of the information bottleneck objective. The reparameterization trick [18] allows the use of deep neural networks to parameterize the distribution to process high-dimensional continuous data.

3 Method: Cell Variational Information Bottleneck

This paper proposes VIB cell which includes distributional representation and KL-divergence regularization in a repeatable small cell.

3.1 Distributional Representation

Specifically, we define a hidden layer $\tilde{\mathbf{x}}$ of input $\mathbf{x}$ as a Gaussian distribution,

$$p(\tilde{\mathbf{x}}|\mathbf{x}) = \mathcal{N}(\tilde{\mathbf{x}};\ \tilde{\mathbf{x}}_\mu,\ \tilde{\mathbf{x}}_\sigma^2\mathrm{I}). \tag{1}$$

The two parameters of the Gaussian distribution, *i.e.*, mean $\tilde{\mathbf{x}}_\mu$ and variance $\tilde{\mathbf{x}}_\sigma$, are both predicted by CNN and related to the input:

$$\tilde{\mathbf{x}}_\mu = f_{\theta_\mu}(\mathbf{x}); \quad \tilde{\mathbf{x}}_\sigma = f_{\theta_\sigma}(\mathbf{x}), \tag{2}$$

where θ_μ and θ_σ refer to the model parameters with respect to output $\tilde{\mathbf{x}}_\mu$ and $\tilde{\mathbf{x}}_\sigma$ respectively. The predicted Gaussian distribution is a diagonal multivariate normal distribution and feature maps of each sample is no longer deterministic, but randomly sampled from $\mathcal{N}(\tilde{\mathbf{x}}; \tilde{\mathbf{x}}_\mu, \tilde{\mathbf{x}}_\sigma^2\mathrm{I})$. However, the sampling operation is not differentiable, thereby preventing the backpropagation of the gradient flow during training. We use the reparameterization technique [18] to make the model still use gradients as usual. Specifically, we first sample a random noise ϵ independent of the model parameters from $\mathcal{N}(\mathbf{0}, \mathrm{I})$, and then treat $\tilde{\mathbf{x}}$ as an equivalent sampling feature map. That is,

$$\tilde{\mathbf{x}} = \tilde{\mathbf{x}}_\mu + \epsilon\tilde{\mathbf{x}}_\sigma, \quad \epsilon \sim \mathcal{N}(\mathbf{0}, \mathrm{I}). \tag{3}$$

The basic structure of cellVIB net is shown in Figure 2. For any given transformation $\mathbf{F}_\mu : \mathbf{X} \to \tilde{\mathbf{X}}_\mu, \mathbf{X} \in \mathbb{R}^{H\times W\times C}, \tilde{\mathbf{X}}_\mu \in \mathbb{R}^{\tilde{H}\times\tilde{W}\times\tilde{C}}$ (for example, a convolutional layer or a convolutional block composed of a series of convolutions), we can construct a corresponding VIB cell as shown below. First, introduce a new transformation $\mathbf{F}_\sigma : \mathbf{X} \to \tilde{\mathbf{X}}_\sigma, \mathbf{X} \in \mathbb{R}^{H\times W\times C}, \tilde{\mathbf{X}}_\sigma \in \mathbb{R}^{\tilde{H}\times\tilde{W}\times\tilde{C}}$, the complexity of $\mathbf{F}_\sigma$ can be lower than $\mathbf{F}_\mu$ to obtain another feature map equal in size to $\mathbf{X}_\mu$ as the standard deviation term. Second, we sample E on a normal distribution. Finally, we input feature maps $\tilde{\mathbf{X}} = \tilde{\mathbf{X}}_\mu + E \cdot \tilde{\mathbf{X}}_\sigma$ into the subsequent layers.

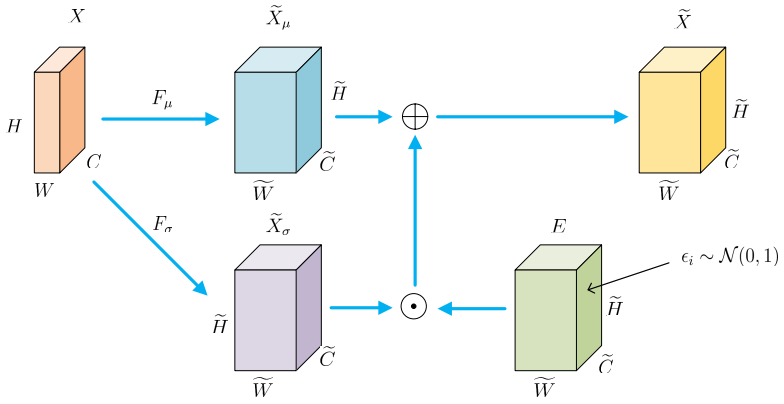

Fig. 2: One variational information bottleneck cell. Best viewed in color.

3.2 KL-Divergence Regularization

Eq. (3) shows that during the training process, feature map $\tilde{\mathbf{x}}_\mu$ is affected by $\tilde{\mathbf{x}}_\sigma$, which will prompt the model to predict a small $\tilde{\mathbf{x}}_\sigma$ for all samples to suppress the unstable component in $\tilde{\mathbf{x}}$. In this case, the random feature map will degrade to $\tilde{\mathbf{x}} = \tilde{\mathbf{x}}_\mu$, which is actually the original deterministic feature map. Inspired by the variational information bottleneck [3], we explicitly constrain $\mathcal{N}(\tilde{\mathbf{x}}_\mu, \tilde{\mathbf{x}}_\sigma^2)$ in the optimization process to make it close to the normal distribution $\mathcal{N}(\mathbf{0}, \mathrm{I})$, measuring by the Kullback-Leibler divergence D_{kl} between them. The Kullback-Leibler divergence term can be written as:

$$\mathcal{L}_{kl} = D_{kl}[\mathcal{N}(\tilde{\mathbf{x}}|\tilde{\mathbf{x}}_\mu, \tilde{\mathbf{x}}_\sigma^2) \,||\, \mathcal{N}(\epsilon|\mathbf{0}, \mathrm{I})]. \tag{4}$$

In Eq. (4), $\mathcal{L}_{kl}$ serves as one good balancer. In particular, only $\tilde{\mathbf{x}}$ is not encouraged to predict the large variance of all samples, which may lead to extreme deterioration of $\tilde{\mathbf{x}}_\mu$, making it difficult for the model to converge. At the same time, $\tilde{\mathbf{x}}$ is not encouraged to predict low variance over all samples, which may in turn lead to one larger $\mathcal{L}_{kl}$ penalty.

3.3 Variational Information Bottleneck in Cell

The input variable of one neural network with I layers is represented as $\mathbf{x}$, and the related target output is represented as $\mathbf{y}$. We denote the activation of the hidden layer of the network as $\{\tilde{\mathbf{x}}_i\}_{i=1}^I$.

Now the feedforward network layer can be interpreted as a Markov chain of successive representation [38], that is,

$$\mathbf{y} \to \mathbf{x} \to \tilde{\mathbf{x}}_1 \to ... \to \tilde{\mathbf{x}}_I \to \hat{\mathbf{y}} \tag{5}$$

Every hidden layer in the network defines a conditional probability $p(\tilde{\mathbf{x}}_i|\tilde{\mathbf{x}}_{i-1})$. For convenience, we use $\mathbf{x} = \tilde{\mathbf{x}}_0$ and $\mathbf{z} = \tilde{\mathbf{x}}_I$.

For the deterministic network model, $p(\tilde{\mathbf{x}}_i|\tilde{\mathbf{x}}_{i-1})$ is absolutely certain. In this situation, the role of the hidden layer is to extract information from the previous layer, while the output layer tries to approximate the real distribution $p(\mathbf{y}|\tilde{\mathbf{x}}_I)$.

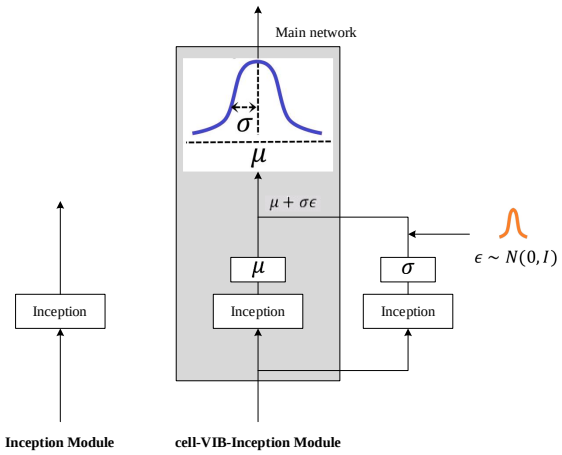

Fig. 3: Left: The Inception Architecture. Right: Our cell-VIB-Inception Module.

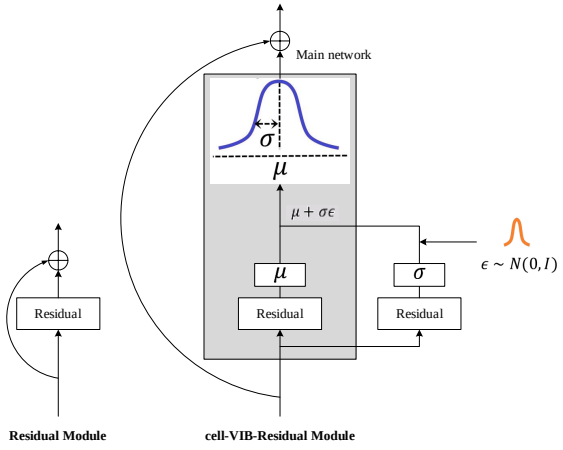

Fig. 4: Left: The Residual Architecture. Right: Our cell-VIB-Residual Module.

Deep VIB introduces a variational information bottleneck in the output layer. On the one hand, it can reduce $I(\tilde{\mathbf{x}}_I, \mathbf{x})$ to remove the redundant content. On the other hand, it can incorporate uncertainty during training. However, only add information bottleneck in the last layer is not sufficient, regardless of to remove redundant information or to add uncertainty. Please see the confirmatory experiments in Figure 5 & Figure 6 (Section 4.1) for detailed discussions.

Our starting point for achieving this goal is to clearly punish the information theory measure of redundancy between each adjacent layer. More specifically, for each hidden layer $\tilde{\mathbf{x}}_i$, we want to minimize the mutual information $I(\tilde{\mathbf{x}}_i, \tilde{\mathbf{x}}_{i-1})$ between $\tilde{\mathbf{x}}_i$ and $\tilde{\mathbf{x}}_{i-1}$, eliminating the redundancy between layers and maximizing the mutual information $I(\tilde{\mathbf{x}}_i, \mathbf{y})$. Therefore, the objective of layer $\mathcal{L}_i$ becomes:

$$\mathcal{L}_i = I(\tilde{\mathbf{x}}_i, \mathbf{y}) - \beta_i I(\tilde{\mathbf{x}}_i, \tilde{\mathbf{x}}_{i-1}). \tag{6}$$

Among them, $\beta_i \geq 0$ is one coefficient, which determines the strength of the bottleneck. To sum each layer, the goal is to minimize $\sum_i \mathcal{L}_i$.

3.4 Applying Cell VIB in Modern Architectures

The flexibility of VIB cells means that they could be directly applied to transformations other than standard convolution. As a result, applying VIB cells to AlexNet [20] or VGGNet [30] is simple. To illustrate this point, we develop cellVIB networks by integrating VIB cells into modern architectures with complex design. For non-residual networks such as the Inception network, as shown in Figure 3, we use an equivalent sampling feature map replacing the entire Inception module to construct the VIB cell. By changing each module in the architecture, we built a cell-VIB-Inception network. Figure 4 describes the architecture of the cell-VIB-ResNet module. An equivalent sampling feature map of VIB cells is treated as a non-identity branch of the residual module. The reparameterization trick works before summing with the identity branch. We describe the architecture of cell-VIB-ResNet-50 in Table 1.

Table 1: Architecture Details for ResNet-50 (left) and Cell-VIB-ResNet-50 (Right). Please see Figure 4 for more detailed descriptions of cell-VIB-Residual module.

Output Size	ResNet-50	cell-VIB-ResNet-50
112×112	conv, 7×7, 64, stride 2	
56×56	max pool, 3×3, 64, stride 2	
56×56	$\begin{pmatrix} 1 \times 1, 64 \\ 3 \times 3, 64 \\ 1 \times 1, 256 \end{pmatrix} \times 3$	$\begin{pmatrix} 1 \times 1, 64+16 \\ 3 \times 3, 64+16 \\ 1 \times 1, 256+256 \end{pmatrix} \times 3$
28×28	$\begin{pmatrix} 1 \times 1, 128 \\ 3 \times 3, 128 \\ 1 \times 1, 512 \end{pmatrix} \times 4$	$\begin{pmatrix} 1 \times 1, 128+32 \\ 3 \times 3, 128+32 \\ 1 \times 1, 512+512 \end{pmatrix} \times 4$
14×14	$\begin{pmatrix} 1 \times 1, 256 \\ 3 \times 3, 256 \\ 1 \times 1, 1024 \end{pmatrix} \times 6$	$\begin{pmatrix} 1 \times 1, 256+64 \\ 3 \times 3, 256+64 \\ 1 \times 1, 1024+1024 \end{pmatrix} \times 6$
7×7	$\begin{pmatrix} 1 \times 1, 512 \\ 3 \times 3, 512 \\ 1 \times 1, 2048 \end{pmatrix} \times 3$	$\begin{pmatrix} 1 \times 1, 512+128 \\ 3 \times 3, 512+128 \\ 1 \times 1, 2048+2048 \end{pmatrix} \times 3$
1×1	average pooling, 7×7, stride 1	
–	FC, softmax	

4 Experiments

4.1 MNIST

Dataset and Architecture. We start with experiments on unmodified MNIST [21] and use the same architecture as [28], namely, an MLP with fully connected layer in the form of "$784-1024-1024-10$", and activated by ReLU.

In our method, each cell in the random encoder has the following form:

$$p(\tilde{x}|x) = \mathcal{N}(\tilde{x}|f_\mu^i(x), \quad f_\sigma^i(x)), \quad i = 1, 2, 3, \tag{7}$$

where i is the depth of the network. Among them, $f_\mu^i(x)$ is the MLP cell with the format of $784-1024$, $1024-1024$, and $1024-K$ respectively, and the output of $f_\mu^3(x)$ is $\tilde{\mathbf{x}}_\mu$, where K is the size of the bottleneck. $f_\sigma^i(x)$ has the same structure as $f_\mu^i(x)$ and outputs encode $\tilde{\mathbf{x}}_\sigma$ after a softplus transform.

Here, we aim to show the advantages of cellVIB in one simple setting, thus we utilize one vanilla classifier architecture. The classifier $f_{cls}(z)$ maps the K-dimensional latent code to the $C = 10$ classes, followed by a simple logistic regression model in the form of $q(y|z) = Softmax(y|f_{cls}(z))$. In the latter part, we will consider more complex architectures in other experiments.

Training. In order to prove that our cellVIB method is advanced compared to the MLP baseline and the original VIB, we here adopt one simple MLP baseline, using a $K = 256$ dimensional bottleneck. During training, we use the Adam optimizer [17], the initial learning rate is $0.0001(\beta_1 = 0.5, \beta_2 = 0.999)$, and exponential decay. The learning rate is decayed by 0.97 every 2 epochs, a

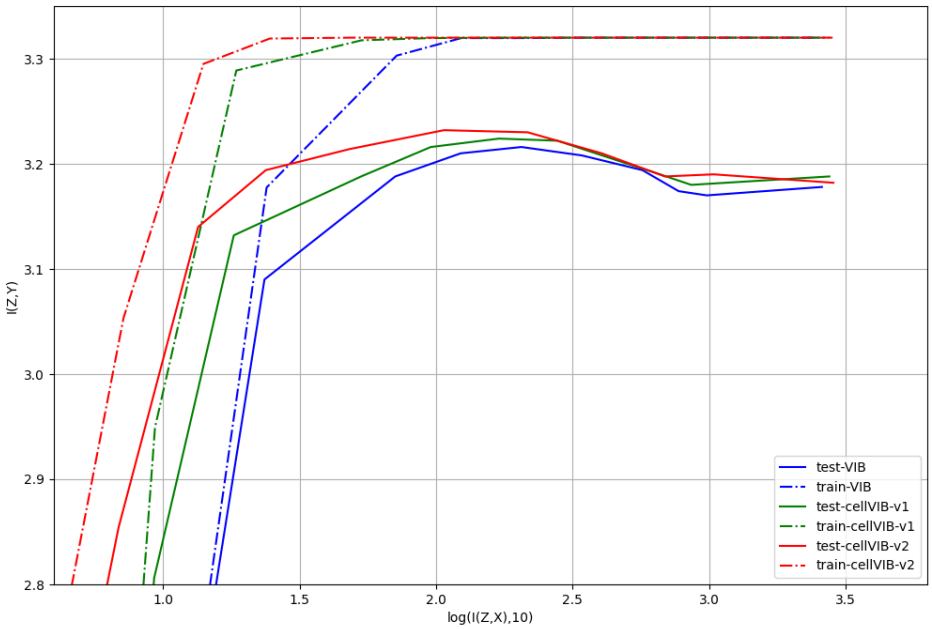

Fig. 5: $I(Z,Y)$ vs $I(Z,X)$ of VIB and cellVIB as we vary β for $K = 256$.

total of 200 training epochs. We use a batch size of 100. 60,000 training and validation images are used for training, and 10,000 test images are used for testing. Before training, we scale the input image to have a value between -1 and 1. The standard deviation is positive through the softplus transformation, and the bias is -5.0, so that they are initially small.

Results and Discussion. In Figure 5, we draw the mutual information curve of original VIB (blue curve), cellVIB-v1 (the second and third fully connected blocks replaced by VIB cells, green curve) and cellVIB-v2 (all fully connected blocks replaced by VIB cells, red curve), *i.e.*, we plot $I(Z,Y)$ vs $I(Z,X)$ as we vary β. Notice that the x-axis is a logarithimc one.

We can observe that the three different structures have some common characteristics. When we allow more information from the input to the bottleneck (by reducing β), the mutual information between the embedding and the labels increases on the training set, but not necessarily on the testing set. In other words, increasing $I(Z,X)$ helps the performance of the training set, but may lead to overfitting, which can be clearly seen from Figure 5.

On the other hand, we can observe that as the original fully connected blocks are replaced by VIB cells gradually, the regularization effect of the network becomes stronger. In three different structures, when $I(Z,X)$, the upper bound on the mutual information between the images X and the stochastic encoding Z, is equal, the $I(Z,Y)$ value of cellVIB-v2 is greater, that is, the mutual information between encoding Z and label Y is greater, and the $I(Z,Y)$ value of the original VIB is the smallest. It can be seen from Eq. (6) that cellVIB is obviously easier to achieve a more ideal optimization state compared to the original VIB.

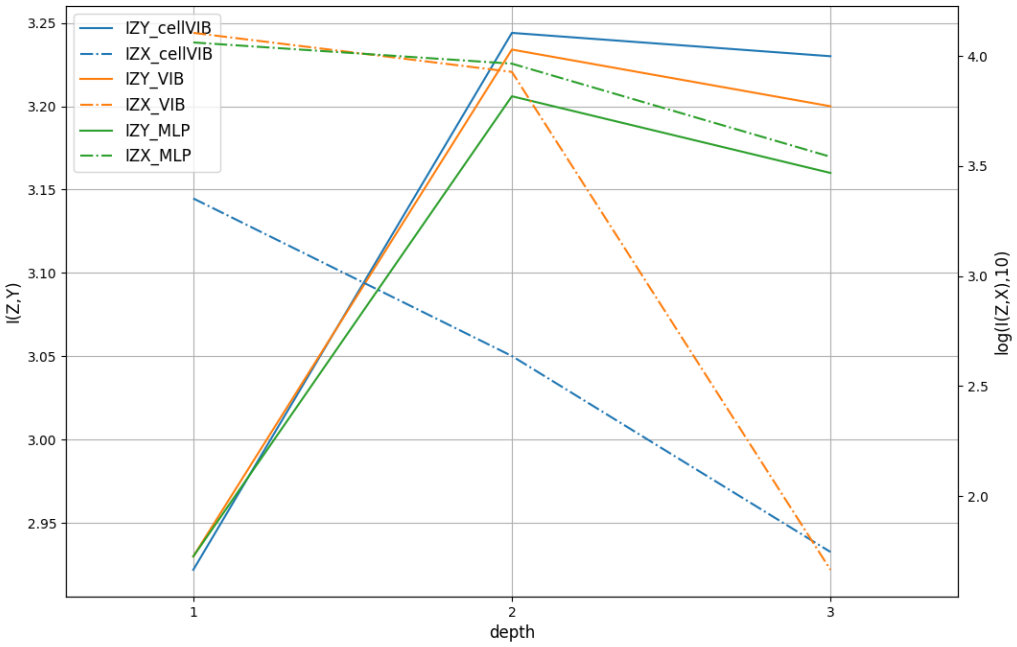

Fig. 6: $I(Z,X)$ and $I(Z,Y)$ vs. *depth* of MLP, VIB and cellVIB for $K = 256$.

We compare our method with the baseline MLP and the baseline variation information bottleneck model [3]. We also consider the following deterministic limitations of the model. When $\beta_i \to 0 (i = 1, 2, 3)$, we observe that the cellVIB optimization process tends to make $f_\sigma^i(x) \to 0 (i = 1, 2, 3)$, so the network becomes nearly deterministic. When $\beta_i \to 0 (i = 1, 2)$, we observe that cellVIB degenerates to the original VIB form, at this time, $f_\sigma^i(x) \to 0 (i = 1, 2)$.

According to the above approximation effect, we draw the changes of $I(Z,Y)$ and $I(Z,X)$ in the test phase with the network depth of MLP, VIB and cellVIB respectively, as illustrated in Figure 6. For the MLP network, since there is no explicit regularization constraint, $I(Z,X)$ only slightly decreases with depth, while $I(Z,Y)$ increases significantly after passing through the second layer of the network and reaches the maximum, and then decreases after passing through the third layer of the network. For the VIB network, since the network only has regularization constraint in the final output layer, $I(Z,X)$ has a similar trend to MLP when passing the first two blocks, and it drops significantly after passing the third layer. At the same time, $I(Z,Y)$ of VIB has the same trend compared to MLP, but larger than MLP due to the influence of regularization constraint. For the cellVIB network, due to the global regularization constraints of the network, $I(Z,X)$ declines in a more gentle trend and reaches a value close to VIB in the output layer, and $I(Z,Y)$ of cellVIB is the largest of the three models.

4.2 Experiments for Robustness

In this section, we evaluate the robustness of the cellVIB model. In image classification tasks, the robustness of the model during training and testing is equally

Table 2: The Averaged Top-1 Accuracy Under 5 Severity Levels. Lv indicates the Level, while ↑ refers to the performance boost. Our cellVIB is superior to the competitors (WRN and Deep VIB) by one large margin, strengthening the model's robustness. In addition, as the severity increases, the gain is more significant.

Method	Lv-1	Lv-2	Lv-3	Lv-4	Lv-5
WRN [44]	85.9	79.0	73.1	65.9	53.8
Deep VIB [3]	86.4	79.6	73.7	66.8	54.7
cellVIB	**88.5**	**81.2**	**75.5**	**68.7**	**56.8**
↑ WRN	2.6	2.2	2.4	2.8	3.0
↑ Deep VIB	2.1	1.6	1.8	1.9	2.1

important. For the robustness of the model in the training phase, we consider label flipping, that is, the situation where images are mislabeled in the training set; for the robustness of the model in the testing phase, we apply different levels and types of corruption to the test images. Without loss of generality, we conduct these experiments in the CIFAR-10 dataset.

Datasets & Architecture. For the task of image classification, CIAFR-10 [19] is a widely-used benchmark. It contains 60000 color images of 10 classes, with 50000 for training and 10000 for testing. The resolution of each image is 32×32. CIFAR-10-C [11] is a corrupted version of CIFAR-10 test set, in which the images are processed by 19 corruption types falling into four main categories: weather, noise, blur and digital. Each corruption contains 5 severity levels, ranging from the lowest level "1" to the highest level "5".

We follow the settings in the Wide Residual Networks (WRN) [44] with 16 layers and the width is 4. The training images are zero-padded by 4 pixels and randomly cropped to 32×32. All the input data subtracts a mean value and is divided by standard deviation per channel for normalization. SGD with a momentum of 0.9 is adopted for the optimization, the batch size is set to 128 and we train the network for 200 epochs. Learning rate is initialized to 0.1 and divided by 5 at 60, 120 and 160 epochs. We conduct all the experiments on two GPUs with Pytorch deep learning framework.

Testing Image Corruption. We train the network on CIFAR-10 training set and report the averaged Top-1 accuracy under 5 severity levels on the CIFAR-10-C. WRN can be viewed as the baseline model, VIB and our proposed cellVIB are based on the WRN architecture, the results are summarized in Table 2.

As shown in Table 2, both VIB and cellVIB outperform the baseline method, indicating that VIB method can enhance the robustness in the testing phase. Moreover, the proposed cellVIB is superior to VIB by one large margin, which suggests that cellVIB has natural advantages in strengthening the model's robustness against the corruption of test images.

Training Label Flips. In the real-world classification scenario, labeling huge dataset for training is laborious and costly. An alternative approach is collecting

Table 3: Top-1 Accuracy on CIFAR-10 Test Set Under Various Noise Levels. WRN collapses rapidly as the noise level increases, while Deep VIB slightly resist the noisy label in the training set. Generally speaking, our cellVIB demonstrates the noise resistant property over these two competitors.

Noise Level	0%	10%	30%	50%	70%
WRN [44]	95.00	90.41	87.81	82.52	69.62
Deep VIB [3]	95.08	91.02	87.98	83.24	70.72
cellVIB	**95.12**	**92.03**	**89.54**	**85.17**	**72.55**
↑ WRN	0.12	1.62	1.73	2.65	2.93
↑ Deep VIB	0.04	1.01	1.56	1.93	1.83

some noisy dataset with keyword searching, allowing some mislabeled example. Hence, we follow the settings of the literature [33] on CIFAR-10 dataset, and set the confusion matrix Q as follows:

$$Q = \begin{pmatrix} 1-r & \frac{r}{9} & \cdots & \frac{r}{9} \\ \frac{r}{9} & 1-r & \cdots & \frac{r}{9} \\ \vdots & \vdots & \ddots & \vdots \\ \frac{r}{9} & \frac{r}{9} & \cdots & 1-r \end{pmatrix}_{10\times 10} \tag{8}$$

where r refers to the mislabeled ratio in the training set. We compare cellVIB with WRN and VIB under various noisy level r, demonstrating the noise resistant property of our proposed method. Top-1 accuracy is reported in Table 3.

The results suggest that both VIB and cellVIB are able to resist the noisy label in the training set while baseline model collapses rapidly as the noise level increases. For example, when the noise level reaches to 70%, the accuracy of WRN drops to 69.62%, while VIB and cellVIB have a higher accuracy of 70.72% and 72.55% respectively. Still, cellVIB outperforms VIB by 1.83% at 70% noise level, indicating that cellVIB is more powerful in resisting training label noise.

How cellVIB Enhance Robustness of Models? As stated in [2], VIB introduces uncertainty in the feature layer, which has two implications for robustness. First, for the noise of the image, regardless of the type of noise, the errors all increase with the norm of the weight matrix through error propagation [39], and there is a definite upper bound. Second, for label noise, the uncertainty introduced by VIB in the feature layer is reflected in the logits. When calculating the loss function (such as cross entropy, etc.) with the label, the effect is actually equivalent to the soft label, being positive to the robustness of label noise.

As demonstrated in the literature [39], in joint perturbation, the upper bound of the predicted label probability difference is larger for full-layer perturbation compared to single-layer perturbation, which shows one conclusions: the cellVIB module has stronger robustness to both image noise and label noise. This conclusions is also consistent with our experimental results.

Table 4: The Top-1 Accuracy (%) on PACAS test set. Our cellVIB has better performance than Deep VIB, further improving the model generalization.

Domain	Art Painting	Cartoon	Photo	Sketch	Ave
baseline	83.61	78.18	94.94	78.22	83.74
Deep VIB [3]	85.30	78.02	**95.68**	77.22	84.05
cellVIB	**85.47**	**78.42**	95.60	**78.46**	**84.49**
↑ baseline	1.86	0.24	0.66	0.24	0.75
↑ Deep VIB	0.17	0.40	-0.08	1.24	0.44

4.3 Experiments for Generalization

Datasets & Architecture. We also conduct experiments on the PACS dataset [22] to demonstrate that cell VIB performs well in generalization. As a commonly used domain generalization benchmark, PACS has dramatic inter-domain shift across four domains: Art Painting, Cartoon, Photo, and Sketch. It consists of 9991 images in 7 common categories: "dog", "elephant", "giraffe", "guitar", "horse", "house" and "person". Generalization of algorithms is measured by training on any three of the four domains and testing on the rest one. Following [22], we randomly choose 20% images from the training domains as validation set. We take the ImageNet pre-trained ResNet-18 as one base model, and then finetune the whole network on the training domains.

Training & Hyperparameter. To match the number of classes for PACS, we replace the fully connected layer and initialize the weights randomly. In VIB model, we add combination of a convolution layer and a BN layer to the end of the last residual block to predict standard deviation.

We use one batch size of 32 images per source domain over the 5k iterations. We optimize the network parameters using SGD with a momentum 0.9, and an initial learning rate $5e-5$. Standard deviation predicting convolution layer in VIB has a 7×7 kernel size with $stride = 1$ and $padding = 0$. Actually it works like a Pooling layer but its parameters are trainable. The variational information bottleneck hyperparameter β is set as 0.001.

Results & Discussion. In Table 4, we compare our method with Deep VIB [3]. One clear tread is concluded: in most domains, except for "photo", our method has better performance than VIB, which shows that cellVIB does help to further improve the generalization performance of the model.

Besides that, the better generalization performance of cellVIB could be explained from two perspectives. First, the regularization introduced between feature maps further reduces the information redundancy between layers, making the mutual information between the final representation Z and the input X smaller. Second, the uncertainty introduced between feature maps makes it difficult for the model to overfit on the training set, therefore forcing the model to learn one more general representation.

4.4 Representation Learning

Datasets & Architecture. We use a cleaned version of MS-Celeb-1M datasets [8] as our training set, containING 3,648,176 images in 79,891 identities. Note that we follow the lists [40, 41] to remove the overlapped identities between the employed training datasets and the test datasets. 2 benchmarks including LFW [13] and Agedb-30 [27], 3 unconstrained benchmarks: CFP [29][1], IJB-B [42] and IJB-C [25], and 2 renovations of LFW: CALFW [46] and CPLFW [45], are used to evaluate our performance following the standard protocols.

We construct one face image (112×112) by warping a face region using three facial points: the two eyes and the midpoint of the two corners of the mouth. We employ the modified 100-layer ResNet [9] as the backbone network. The head of the baseline model is: BackBone-Flatten-FC-BN with embedding dimensions of 512 and dropout probability of 0.4 to output the embedding feature.

Training & Hyperparameter. We use 8 GPUs with Pytorch deep learning framework to train the baseline model and cellVIB, with batch sizes of 512 and 200k steps. We use an initial learning rate of 0.1, and use a stochastic gradient descent (SGD) optimizer to reduce the learning rate by 0.1 at 100k, 140k, and 160k with a weight decay of 0.0001 and a momentum of 0.9. For the cellVIB model, we set the trade-off hyperparameter β_i to uniformly decrease with the depth i, the maximum β_i is 0.001, and the minimum β_i is 0.

Compared Methods. The original ArcFace [6] is used as the baseline. In addition, we compared our method with the original Deep VIB. In the training process, both the embedding features and the weights in the classifier are L2-normalized, and cosine similarity is used for evaluation. We re-implement these methods in accordance with every detail in the original literature, and make fair comparisons under the same experimental settings.

Evaluation on General Datasets. We compare with the baseline and Deep VIB on the general face recognition test set (that is, the test set with limited changes within the group). Table 5 summarizes the results of these evaluations. It is worth noting that on these test sets, the performance of the baseline model has almost reached saturation, and the advantages of cellVIB are not obvious, but cellVIB still slightly improve the accuracy of some of the test sets.

Evaluation on Mixed-Quality Datasets. When evaluating on the challenging datasets, such as IJB-B and IJB-C, these datasets have a large domain gap with high-quality training datasets. At this time, the cellVIB model has better performance compared with the baseline model and Deep VIB, especially when the false acceptance rate is low, as shown in the Table 5.

Discussion. In most benchmark tests, our proposed method outperforms the benchmark deterministic model. These results show that, compared with the point embedding estimated by the baseline model and the normal distribution of a single sample estimated by Deep VIB, embedding estimated by feature maps

[1] Noted that we only use "frontal-profile" protocol of CFP

Table 5: Results of ResNet100 models trained on MS-Celeb-1M. The ArcFace model outputs a deterministic embeddings. The better performance among each base model are shown in bold numbers. Our cellVIB performs better than ArcFace and Deep VIB, especially when the false acceptance rate is low.

Method	LFW	CFP-FP	CALFW	CPLFW	Agedb-30	
ArcFace [6]	99.77	98.14	96.10	92.77	92.77	
Deep VIB [3]	99.78	98.07	**96.18**	92.58	**98.08**	
cellVIB	**99.83**	**98.27**	96.14	**92.85**	**98.08**	
Method	IJB-B(TPR@FPR)			IJB-C(TPR@FPR)		
	0.001%	0.01%	0.1%	0.001%	0.01%	0.1%
ArcFace [6]	88.97	94.72	96.59	93.54	96.11	**97.51**
Deep VIB [3]	87.69	94.74	96.47	93.75	96.08	97.41
cellVIB	**89.65**	**94.82**	**96.63**	**93.94**	**96.15**	97.46

with uncertainty has better intra-class compactness and inter-class separability, especially in unconstrained benchmarks: such as CFP with front/side photos, and IJB-C which contains blurred photos collected from YouTube videos. CellVIB has made the most significant progress in the IJB benchmark verification protocol, which is also the most challenging one. This phenomenon reveals that the model with uncertainty is more suitable for unconstrained face recognition scenarios than the deterministic model.

It is worth mentioning that, in the current face recognition task, because the number of hyperparameters in cellVIB is very large, and the hyperparameters are all artificially set, cellVIB may still not achieve the best performance in the above-mentioned backbone. We will try to use reinforcement learning to explore the automatic setting of β_i in our future work. And we believe this could further improve the performance of cellVIB in complex models.

5 Conclusion

We propose Cell Variational Information Bottleneck (cellVIB), which has a novel cell structure, being able to directly replace the intermediate structure of the existing networks. We use a distribution to replace the original feature maps during training, so that the information redundancy between layers is less, and the uncertainty during training is more. Extensive experiments have proved the effectiveness of our cellVIB, which achieve competitive performance on multiple different tasks and datasets. In addition, cellVIB also has better robustness and generalization, and has strong adaptability to noisy data or labels and unknown domains. In future work, we will further explore ways to reduce the number of hyperparameters or use reinforcement learning to automatically learn hyperparameters to further improve the practicality of our model.

References

1. Agakov, D.B.F.: The im algorithm: a variational approach to information maximization. Advances in neural information processing systems **16**, 201 (2004) 4
2. Alemi, A.A., Fischer, I., Dillon, J.V.: Uncertainty in the variational information bottleneck. arXiv preprint arXiv:1807.00906 (2018) 2, 11
3. Alemi, A.A., Fischer, I., Dillon, J.V., Murphy, K.: Deep variational information bottleneck. arXiv preprint arXiv:1612.00410 (2016) 1, 4, 5, 9, 10, 11, 12, 14
4. Chechik, G., Globerson, A., Tishby, N., Weiss, Y., Dayan, P.: Information bottleneck for gaussian variables. Journal of machine learning research **6**(1) (2005) 1
5. Chollet, F.: Xception: Deep learning with depthwise separable convolutions. In: Proceedings of the IEEE conference on computer vision and pattern recognition. pp. 1251–1258 (2017) 3
6. Deng, J., Guo, J., Xue, N., Zafeiriou, S.: Arcface: Additive angular margin loss for deep face recognition. In: Proceedings of the IEEE/CVF Conference on Computer Vision and Pattern Recognition. pp. 4690–4699 (2019) 13, 14
7. Ghiasi, G., Lin, T.Y., Le, Q.V.: Dropblock: A regularization method for convolutional networks. arXiv preprint arXiv:1810.12890 (2018) 3
8. Guo, Y., Zhang, L., Hu, Y., He, X., Gao, J.: Ms-celeb-1m: A dataset and benchmark for large-scale face recognition. In: European conference on computer vision. pp. 87–102. Springer (2016) 13
9. He, K., Zhang, X., Ren, S., Sun, J.: Deep residual learning for image recognition. In: Proceedings of the IEEE conference on computer vision and pattern recognition. pp. 770–778 (2016) 3, 13
10. He, K., Zhang, X., Ren, S., Sun, J.: Identity mappings in deep residual networks. In: European conference on computer vision. pp. 630–645. Springer (2016) 3
11. Hendrycks, D., Dietterich, T.: Benchmarking neural network robustness to common corruptions and perturbations. Proceedings of the International Conference on Learning Representations (2019) 10
12. Higgins, I., Matthey, L., Pal, A., Burgess, C., Glorot, X., Botvinick, M., Mohamed, S., Lerchner, A.: beta-vae: Learning basic visual concepts with a constrained variational framework. In: International conference on learning representations (2016) 4
13. Huang, G.B., Mattar, M., Berg, T., Learned-Miller, E.: Labeled faces in the wild: A database forstudying face recognition in unconstrained environments. In: Workshop on faces in'Real-Life'Images: detection, alignment, and recognition (2008) 13
14. Ioannou, Y., Robertson, D., Cipolla, R., Criminisi, A.: Deep roots: Improving cnn efficiency with hierarchical filter groups. In: Proceedings of the IEEE conference on computer vision and pattern recognition. pp. 1231–1240 (2017) 3
15. Ioffe, S., Szegedy, C.: Batch normalization: Accelerating deep network training by reducing internal covariate shift. In: International conference on machine learning. pp. 448–456. PMLR (2015) 3
16. Jaderberg, M., Vedaldi, A., Zisserman, A.: Speeding up convolutional neural networks with low rank expansions. arXiv preprint arXiv:1405.3866 (2014) 3
17. Kingma, D.P., Ba, J.: Adam: A method for stochastic optimization. arXiv preprint arXiv:1412.6980 (2014) 7
18. Kingma, D.P., Welling, M.: Auto-encoding variational bayes. arXiv preprint arXiv:1312.6114 (2013) 1, 4

19. Krizhevsky, A., Hinton, G., et al.: Learning multiple layers of features from tiny images (2009) 10
20. Krizhevsky, A., Sutskever, I., Hinton, G.E.: Imagenet classification with deep convolutional neural networks. Advances in neural information processing systems **25**, 1097–1105 (2012) 6
21. LeCun, Y., Bottou, L., Bengio, Y., Haffner, P.: Gradient-based learning applied to document recognition. Proceedings of the IEEE **86**(11), 2278–2324 (1998) 7
22. Li, D., Yang, Y., Song, Y.Z., Hospedales, T.M.: Deeper, broader and artier domain generalization. In: Proceedings of the IEEE international conference on computer vision. pp. 5542–5550 (2017) 12
23. Lin, M., Chen, Q., Yan, S.: Network in network. arXiv preprint arXiv:1312.4400 (2013) 3
24. Liu, H., Simonyan, K., Vinyals, O., Fernando, C., Kavukcuoglu, K.: Hierarchical representations for efficient architecture search. arXiv preprint arXiv:1711.00436 (2017) 3
25. Maze, B., Adams, J., Duncan, J.A., Kalka, N., Miller, T., Otto, C., Jain, A.K., Niggel, W.T., Anderson, J., Cheney, J., et al.: Iarpa janus benchmark-c: Face dataset and protocol. In: 2018 International Conference on Biometrics (ICB). pp. 158–165. IEEE (2018) 13
26. Mohamed, S., Rezende, D.J.: Variational information maximisation for intrinsically motivated reinforcement learning. arXiv preprint arXiv:1509.08731 (2015) 4
27. Moschoglou, S., Papaioannou, A., Sagonas, C., Deng, J., Kotsia, I., Zafeiriou, S.: Agedb: the first manually collected, in-the-wild age database. In: Proceedings of the IEEE Conference on Computer Vision and Pattern Recognition Workshops. pp. 51–59 (2017) 13
28. Pereyra, G., Tucker, G., Chorowski, J., Kaiser, Ł., Hinton, G.: Regularizing neural networks by penalizing confident output distributions. arXiv preprint arXiv:1701.06548 (2017) 7
29. Sengupta, S., Chen, J.C., Castillo, C., Patel, V.M., Chellappa, R., Jacobs, D.W.: Frontal to profile face verification in the wild. In: 2016 IEEE Winter Conference on Applications of Computer Vision (WACV). pp. 1–9. IEEE (2016) 13
30. Simonyan, K., Zisserman, A.: Very deep convolutional networks for large-scale image recognition. arXiv preprint arXiv:1409.1556 (2014) 3, 6
31. Srivastava, N., Hinton, G., Krizhevsky, A., Sutskever, I., Salakhutdinov, R.: Dropout: a simple way to prevent neural networks from overfitting. The journal of machine learning research **15**(1), 1929–1958 (2014) 3
32. Srivastava, R.K., Greff, K., Schmidhuber, J.: Training very deep networks. arXiv preprint arXiv:1507.06228 (2015) 3
33. Sukhbaatar, S., Bruna, J., Paluri, M., Bourdev, L., Fergus, R.: Training convolutional networks with noisy labels. arXiv preprint arXiv:1406.2080 (2014) 11
34. Szegedy, C., Ioffe, S., Vanhoucke, V., Alemi, A.: Inception-v4, inception-resnet and the impact of residual connections on learning. In: Proceedings of the AAAI Conference on Artificial Intelligence (2017) 3
35. Szegedy, C., Liu, W., Jia, Y., Sermanet, P., Reed, S., Anguelov, D., Erhan, D., Vanhoucke, V., Rabinovich, A.: Going deeper with convolutions. In: Proceedings of the IEEE conference on computer vision and pattern recognition. pp. 1–9 (2015) 3
36. Szegedy, C., Vanhoucke, V., Ioffe, S., Shlens, J., Wojna, Z.: Rethinking the inception architecture for computer vision. In: Proceedings of the IEEE conference on computer vision and pattern recognition. pp. 2818–2826 (2016) 3

37. Tishby, N., Pereira, F.C., Bialek, W.: The information bottleneck method. arXiv preprint physics/0004057 (2000) 1
38. Tishby, N., Zaslavsky, N.: Deep learning and the information bottleneck principle. In: 2015 IEEE Information Theory Workshop (ITW). pp. 1–5. IEEE (2015) 1, 3, 5
39. Tsai, Y.L., Hsu, C.Y., Yu, C.M., Chen, P.Y.: Non-singular adversarial robustness of neural networks. arXiv preprint arXiv:2102.11935 (2021) 2, 11
40. Wang, X., Wang, S., Wang, J., Shi, H., Mei, T.: Co-mining: Deep face recognition with noisy labels. In: Proceedings of the IEEE international conference on computer vision. pp. 9358–9367 (2019) 13
41. Wang, X., Zhang, S., Wang, S., Fu, T., Shi, H., Mei, T.: Mis-classified vector guided softmax loss for face recognition. arXiv preprint arXiv:1912.00833 (2019) 13
42. Whitelam, C., Taborsky, E., Blanton, A., Maze, B., Adams, J., Miller, T., Kalka, N., Jain, A.K., Duncan, J.A., Allen, K., et al.: Iarpa janus benchmark-b face dataset. In: proceedings of the IEEE conference on computer vision and pattern recognition workshops. pp. 90–98 (2017) 13
43. Xie, S., Girshick, R., Dollár, P., Tu, Z., He, K.: Aggregated residual transformations for deep neural networks. In: Proceedings of the IEEE conference on computer vision and pattern recognition. pp. 1492–1500 (2017) 3
44. Zagoruyko, S., Komodakis, N.: Wide residual networks. arXiv preprint arXiv:1605.07146 (2016) 10, 11
45. Zheng, T., Deng, W.: Cross-pose lfw: A database for studying cross-pose face recognition in unconstrained environments. Beijing University of Posts and Telecommunications, Tech. Rep **5** (2018) 13
46. Zheng, T., Deng, W., Hu, J.: Cross-age lfw: A database for studying cross-age face recognition in unconstrained environments. arXiv preprint arXiv:1708.08197 (2017) 13
47. Zoph, B., Le, Q.V.: Neural architecture search with reinforcement learning. arXiv preprint arXiv:1611.01578 (2016) 3
48. Zoph, B., Vasudevan, V., Shlens, J., Le, Q.V.: Learning transferable architectures for scalable image recognition. In: Proceedings of the IEEE conference on computer vision and pattern recognition. pp. 8697–8710 (2018) 3

Cell Variational Information Bottleneck Network – Supplementary Material

Anonymous ECCV 2024 Submission

Paper ID #10474

In this supplementary material, we present an extended analysis and additional details pertaining to our investigation into the integration of the Cell Variational Information Bottleneck (cellVIB) within the framework of the Vision Transformer (ViT) [**?**]. The intent of this document is to elaborate on the methodologies employed, the architectural enhancements, and the experimental validations that substantiate the claims of our principal publication. Through meticulous modifications to the ViT architecture, introducing stochasticity, and leveraging the principles of regularization, we endeavor to refine the performance and generalizability of deep learning models in visual recognition tasks. Subsequent sections will systematically expound upon the architectural modifications, the rigorous comparative evaluations of varied implementations, and the empirical performance metrics obtained on the ImageNet dataset [**?**], culminating in a comprehensive discussion of the implications and contributions of the cellVIB methodology to the field of machine learning.

1. Integration of cellVIB into ViT Architecture

The cell Variational Information Bottleneck (cellVIB) approach has been incorporated into the Vision Transformer (ViT) architecture to enhance its capacity for managing information flow and to introduce regularization through uncertainty. This section describes the integration process and the results of our empirical analysis on the ImageNet dataset.

1.1. Architecture Modifications in MHA

In the original ViT, each transformer encoder block consists of a Multi-Head Attention (MHA) module followed by a Feed-Forward Network (FFN) module. For the integration of cellVIB, we have employed a dual-branch structure within the MHA component. One branch computes the mean μ, and the other computes the standard deviation σ. Randomness is then introduced by sampling from the Gaussian distribution defined by the predicted mean μ and standard deviation σ. This sampled output is further processed by the typical residual structure found in conventional ViT models (Figure 1).

1.2. Implementation Details and Modifications in FFN

Unlike the MHA component, the FFN part of the ViT architecture has not been modified to include the cellVIB structure. This decision was based on experimental findings, which are discussed in the next section.

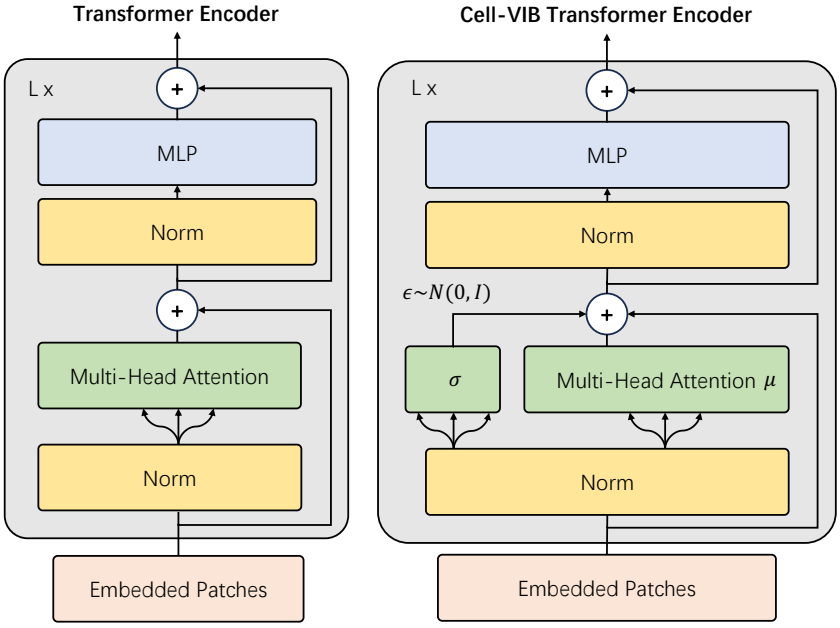

Fig. 1: Cell-VIB Transformer Encoder.

Table 1: Comparison between baseline ViT and ViT-cellVIB on ImageNet(21K+1K). 21K+1K denotes pre-training on ImageNet-21K and finetuning on ImageNet-1K.

Model	Eval Size	Params	FLOPs	Top-1 Accuracy (%)
ViT-L/16	384^2	304M	190.7B	85.3
ViT-cellVIB (MHA + FFN with cellVIB)	384^2	344M	213.6B	86.3
ViT-cellVIB (Only MHA with cellVIB)	384^2	334M	209.8B	**86.9**
ViT-cellVIB (Only FFN with cellVIB)	384^2	314M	194.5B	85.5

2. Empirical Analysis and Comparative Study

We conducted experiments to compare the following configurations: a) both MHA and FFN with cellVIB, b) only MHA with cellVIB, and c) only FFN with cellVIB. The results indicated that configuration b) yielded the best performance. This suggests that the introduction of stochasticity at the attention level offers a more significant benefit than when applied to the feed-forward layers. One possible explanation could be that the attention mechanism is inherently more sensitive to the regularization induced by the uncertainty, which enhances the model's ability to focus on relevant information while ignoring noise.

3. Performance Results on ImageNet

We evaluated the modified ViT architecture with cellVIB integration (ViT-cellVIB) on the ImageNet dataset. Below, we present Table 1 illustrating the comparison between the baseline ViT and ViT-cellVIB.

4. Conclusion

The integration of cellVIB into the ViT architecture has demonstrated the efficacy of selective stochasticity and regularization in improving the robustness and efficacy of attention mechanisms in transformers. The empirical results highlight the potential benefits of cellVIB when applied to the MHA component, paving the way for further exploration and optimization of transformer architectures.